Published in final edited form as:
Biomaterials. 2012 June ; 33(16): 4147–4156. doi:10.1016/j.biomaterials.2012.02.031.

In Vivo Targeting and Positron Emission Tomography Imaging of Tumor Vasculature with ^{66}Ga-Labeled Nano-Graphene

Hao Hong[1,5], **Yin Zhang**[2,5], **Jonathan W. Engle**[2], **Tapas R. Nayak**[1], **Charles P. Theuer**[3], **Robert J. Nickles**[2], **Todd E. Barnhart**[2], and **Weibo Cai**[1,2,4,*]

[1]Department of Radiology, University of Wisconsin - Madison, Madison, WI, USA

[2]Department of Medical Physics, University of Wisconsin - Madison, Madison, WI, USA

[3]TRACON Pharmaceuticals, Inc., San Diego, CA, USA

[4]University of Wisconsin Carbone Cancer Center, Madison, WI, USA

Abstract

The goal of this study was to employ nano-graphene for tumor targeting in an animal tumor model, and quantitatively evaluate the pharmacokinetics and tumor targeting efficacy through positron emission tomography (PET) imaging using ^{66}Ga as the radiolabel. Nano-graphene oxide (GO) sheets with covalently linked, amino group-terminated six-arm branched polyethylene glycol (PEG; 10 kDa) chains were conjugated to NOTA (1,4,7-triazacyclononane-1,4,7-triacetic acid, for ^{66}Ga-labeling) and TRC105 (an antibody that binds to CD105). Flow cytometry analyses, size measurements, and serum stability studies were performed to characterize the GO conjugates before in vivo investigations in 4T1 murine breast tumor-bearing mice, which were further validated by histology. TRC105-conjugated GO was specific for CD105 in cell culture. ^{66}Ga-NOTA-GO-TRC105 and ^{66}Ga-NOTA-GO exhibited excellent stability in complete mouse serum. In 4T1 tumor-bearing mice, these GO conjugates were primarily cleared through the hepatobiliary pathway. ^{66}Ga-NOTA-GO-TRC105 accumulated quickly in the 4T1 tumors and tumor uptake remained stable over time (3.8 ± 0.4, 4.5 ± 0.4, 5.8 ± 0.3, and 4.5 ± 0.4 %ID/g at 0.5, 3, 7, and 24 h post-injection respectively; n = 4). Blocking studies with unconjugated TRC105 confirmed CD105 specificity of ^{66}Ga-NOTA-GO-TRC105, which was corroborated by biodistribution and histology studies. Furthermore, histological examination revealed that targeting of NOTA-GO-TRC105 is tumor vasculature CD105 specific with little extravasation. Successful demonstration of in vivo tumor targeting with GO, along with the versatile chemistry of graphene-based nanomaterials, makes them suitable nanoplatforms for future biomedical research such as cancer theranostics.

Keywords

Graphene; ^{66}Ga; CD105 (endoglin); positron emission tomography (PET); molecular imaging; tumor angiogenesis

Requests for reprints: Weibo Cai, PhD, Departments of Radiology and Medical Physics, University of Wisconsin -Madison, Room 7137, 1111 Highland Avenue, Madison, WI 53705-2275, USA wcai@uwhealth.org; Phone: 608-262-1749; Fax: 608- 265-0614.
[5]The authors contributed equally to this work

The other authors declare that they have no conflict of interest.

1. Introduction

Graphene, a 2-D sp^2-bonded carbon sheet with desirable electrical/mechanical/chemical properties, has attracted enormous interest in biomedicine [1–4]. Recently, functionalized nano-graphene with ultra-high surface area has been used as a nano-carrier for loading and delivery of various drugs and genes [2, 5–7]. In vivo applications of nano-graphene for cancer therapy have been further explored, with encouraging therapeutic effects in animal models [8, 9]. The potential toxicity of graphene has also been investigated [2, 10–13], and it is generally agreed that the toxicity of graphene is closely associated with its surface chemistry. For example, a recent study suggested that polyethylene glycol (PEG) functionalized nano-graphene could be gradually excreted from mice after intravenous injection, without rendering noticeable toxicity to the treated animals [10].

In this study, we explored the use of nano-graphene for in vivo tumor targeting and quantitatively evaluated the pharmacokinetics and tumor targeting efficacy through serial non-invasive positron emission tomography (PET) imaging. To ensure in vivo stability of the nano-graphene conjugates, we used 10–50 nm graphene oxide (GO) sheets with six-arm branched PEG (10 kDa) chains covalently attached to the surfaces [5, 8], which have ample amino groups for covalent conjugation of various functional entities (imaging labels, antibodies, etc.).

Recently, we have produced high specific activity ^{66}Ga ($t_{1/2}$ = 9.3 h, 56.5% β^+, 43.5% EC) from ^{nat}Znand ^{66}Zn targets with a cyclotron, using proton irradiations between 7 and 16 MeV. The reactivities of ^{66}Ga for common bifunctional chelators exceeded 70 GBq/μmol [14], which were significantly higher than the previously reported values (< 4.6 GBq/μmol) [15]. The relatively long half-life of ^{66}Ga makes it a suitable radiolabel for nanomaterials such as GO, whose in vivo kinetics is poorly matched by the much shorter half-life of ^{68}Ga ($t_{1/2}$ = 68.3 min). Labeling chemistry with radiogallium has been well studied because of the popularity of ^{68}Ga from ^{68}Ge/^{68}Ga generators, and 1,4,7-triazacyclononane-1,4,7-triacetic acid (NOTA) is generally agreed to be one of the most suitable chelators [16].

Almost exclusively expressed on proliferating tumor endothelial cells, CD105 (endoglin) is an ideal marker for tumor angiogenesis (i.e. new blood vessel formation) [17–19]. It holds tremendous clinical potential as a prognostic, diagnostic, and therapeutic vascular target in cancer, since high expression level of CD105 correlates with poor prognosis in more than 10 solid tumor types [20]. In addition, the fact that CD105 is not readily detectable in resting endothelial cells or most normal organs makes it a universally applicable target for molecular imaging and therapy applications targeting the tumor vasculature. For most nanomaterial-based tumor targeting and imaging, efficient extravasation is the key hurdle [21, 22]. In this regard, CD105 is highly desirable for nanomaterial-based tumor targeting, such as the functionalized GO used in this study, where extravasation is not required to observe the tumor signal.

TRC105, a human/murine chimeric IgG1 monoclonal antibody (mAb) which binds to CD105 with high avidity, is used here as the targeting ligand for CD105 [17]. A multicenter Phase 1 first-in-human dose-escalation trial of TRC105 was recently completed in the United States and multiple Phase 2 cancer therapy trials are underway [23]. These promising clinical data warranted the development of TRC105-based imaging/therapeutic agents, which can play important roles in multiple facets of future cancer patient management. Therefore, the goal of this study is to investigate whether TRC105 can be used as the ligand for CD105 targeting of covalently functionalized GO in an animal tumor model, which can open up new possibilities for future image-guided drug delivery, cancer therapy, as well as establishing GO as a promising nanoplatform for cancer theranostics. To validate the in vivo

data, various in vitro/in vivo/ex vivo studies and control experiments were carried out to confirm CD105 specificity of the GO conjugates.

2. Materials and methods

2.1. Reagents

TRC105 was provided by TRACON pharmaceuticals Inc. (San Diego, CA). S-2-(4-isothiocyanatobenzyl)-1,4,7-triazacyclononane-1,4,7-triacetic acid (p-SCN-Bn-NOTA) and fluorescein isothiocyanate (FITC) were purchased from Macrocyclics, Inc. (Dallas, TX) and Sigma-Aldrich (St. Louis, MO) respectively. Chelex 100 resin (50–100 mesh; Sigma-Aldrich, St. Louis, MO), succinimidyl carboxymethyl PEG maleimide (SCM-PEG-Mal, molecular weight: 5 kDa; Creative PEGworks, Winston Salem, NC), rat anti-mouse CD31 primary antibody (BD Biosciences, San Diego, CA), AlexaFluor488- and Cy3-labeled secondary antibodies (Jackson Immunoresearch Laboratories, Inc., West Grove, CA), and PD-10 desalting columns (GE Healthcare, Piscataway, NJ) were all acquired from commercial sources. Water and all buffers were of Millipore grade and pre-treated with Chelex 100 resin to ensure that the aqueous solution was heavy metal-free. All other reaction buffers and chemicals were obtained from Thermo Fisher Scientific (Fair Lawn, NJ).

2.2. Cell lines and animal model

4T1 murine breast cancer, MCF-7 human breast cancer, and human umbilical vein endothelial cells (HUVECs) were purchased from the American Type Culture Collection (ATCC, Manassas, VA). 4T1 and MCF-7 cells were cultured in RPMI 1640 medium (Invitrogen, Carlsbad, CA) with 10% fetal bovine serum and incubated at 37 °C with 5% CO_2. HUVECs were cultured in M-200 medium (Invitrogen, Carlsbad, CA) with 1× low serum growth supplement (Cascade Biologics, Portland, OR) and incubated at 37 °C with 5% CO_2. Cells were used for in vitro and in vivo experiments when they reached ~75% confluence.

All animal studies were conducted under a protocol approved by the University of Wisconsin Institutional Animal Care and Use Committee. Four- to five-week-old female BALB/c mice were purchased from Harlan (Indianapolis, IN) and 4T1 tumors were established by subcutaneously injecting 2×10^6 cells, suspended in 100 μL of 1:1 mixture of RPMI 1640 medium and Matrigel (BD Biosciences, Franklin lakes, NJ), into the front flank of mice. Tumor sizes were monitored every other day and mice were used for in vivo experiments when the diameter of tumors reached 5–8 mm.

2.3. Syntheses and characterization of GO conjugates

The synthesis of PEGylated GO (termed "GO-PEG-NH_2"), starting from graphite oxide, has been reported previously [5, 8]. Four conjugates of GO-PEG-NH_2 were prepared and investigated in this study: NOTA-GO, NOTA-GO-TRC105, FITC-GO, and FITC-GO-TRC105 (Figure 1A). Since all conjugates contain the same six-arm branched PEG chains covalently linked to GO, "PEG" was omitted from the acronyms for clarity considerations. NOTA-GO and NOTA-GO-TRC105 were subsequently labeled with ^{66}Ga for in vivo PET imaging and biodistribution studies, while FITC-GO and FITC-GO-TRC105 were employed for in vitro evaluation of CD105 binding affinity and specificity through fluorescence techniques.

GO-PEG-NH_2 was mixed with p-SCN-Bn-NOTA or FITC, which has the same chemical reaction between the SCN group and the -NH_2 group, at a molar ratio of 1:10 at pH 9.0 for 2 h. The resulting NOTA-GO (or FITC-GO) was purified by centrifugation filtration using

100 kDa cutoff Amicon filters (Millipore, Billerica, MA). NOTA-GO (or FITC-GO) was subsequently reacted with SCM-PEG-Mal at pH 8.5 at a molar ratio of 1:30 for 2 h. After removing the unreacted SCM-PEG-Mal and other reagents by centrifugation filtration, the resulting reaction intermediates were named as NOTA-GO-Mal or FITC-GO-Mal.

In parallel, TRC105 was mixed with Traut's reagent at a molar ratio of 1:25 at pH 8.0 for 2 h. The thiolated TRC105 (i.e. TRC105-SH) was purified by size exclusion chromatography using phosphate-buffered saline (PBS, pre-treated with Chelex 100 resin to prevent oxidation of the thiol) as the mobile phase. Subsequently, NOTA-GO-Mal or FITC-GO-Mal was mixed with TRC105-SH at a molar ratio of 1:5 at pH 7.5 in the presence of tris(2-carboxyethyl)phosphine (TCEP; to avoid disulfide formation between TRC105-SH). The final products were purified by centrifugation filtration, which were named NOTA-GO-TRC105 and FITC-GO-TRC105. To characterize the GO conjugates, atom force microscopy (AFM), dynamic light scattering (DLS), and zeta-potential measurements were carried out.

2.4. Production of ^{66}Ga

Targets of ^{nat}Zn or ^{66}Zn were electrodeposited from 0.05 N hydrochloric acid solution onto gold or silver target backings with dimensions approximately matched to the cyclotron beam of a General Electric (Waukesha, WI) PETtrace cyclotron [14]. Targets were irradiated with 20 – 30 μA of 13 MeV protons for between 1 and 3 h, dissolved in concentrated HCl, and purified by cation exchange chromatography with successive additions of 10 N and 7 N HCl to recover the zinc target material and elute trace contaminant metals. The product was collected in 4 N HCl and evaporated to dryness before being redissolved in 0.1 N HCl prior to buffering. If ^{nat}Zn was used as the target, ^{68}Ga was allowed to decay overnight before target processing commenced. In this case, the only radioisotopic contaminant was ^{67}Ga ($t_{1/2}$ = 78.3 h), present as < 5% of the radioactivity at 16 h after the end of bombardment (EoB). On the other hand, radioisotopic purity of ^{66}Ga produced from ^{66}Zn target exceeded 99.9%.

2.5. Radiolabeling of GO conjugates

74–111 MBq of ^{66}Ga-acetate (pH 5.5) was prepared from 0.1 N HCl solution by addition of 0.25 M NH_4OAc solution (pH 7.2), and added to a solution of NOTA-GO-TRC105 or NOTA-GO, at a ratio of 30 μg of each GO conjugate per 37 MBq of ^{66}Ga. The reaction mixture was incubated for 30 min at 37 °C with constant shaking. ^{66}Ga-NOTA-GO-TRC105 and ^{66}Ga-NOTA-GO were purified by size exclusion chromatography using normal saline buffered with 0.25 M NH_4OAc (pH 7.2) as the mobile phase. The radioactive fractions containing ^{66}Ga-NOTA-GO-TRC105 or ^{66}Ga-NOTA-GO were collected and passed through a 0.2 μm syringe filter prior to injection into 4T1 tumor-bearing mice.

2.6. In vitro studies of GO conjugates

To evaluate the CD105-targeting characteristics of the GO conjugates, HUVECs (that express high levels of CD105 [24–26]) and MCF-7 cells (that do not express CD105) were used for flow cytometry analysis of FITC-GO and FITC-GO-TRC105. Cells were harvested and suspended in cold PBS with 2% bovine serum albumin at a concentration of 5×10^6 cells/mL, incubated with FITC-GO-TRC105 or FITC-GO (at a concentration of 50 μg/mL based on GO) for 30 min at room temperature, washed three times with cold PBS, and centrifuged at 1,000 rpm for 5 min. Afterwards, the cells were washed and analyzed using a BD FACSCalibur four-color analysis cytometer, which is equipped with 488 nm and 633 nm lasers (Becton-Dickinson, San Jose, CA). FlowJo analysis software (Tree Star, Ashland, OR) was used to analyze the data. A “blocking” experiment was also performed in cells

incubated with 50 μg/mL of FITC-GO-TRC105, where 500 μg/mL of unconjugated TRC105 was added to evaluate the CD105 specificity of FITC-GO-TRC105.

To ensure that ^{66}Ga-NOTA-GO-TRC105 and ^{66}Ga-NOTA-GO are sufficiently stable for in vivo applications, serum stability studies were carried out where ^{66}Ga-NOTA-GO-TRC105 or ^{66}Ga-NOTA-GO were incubated in complete mouse serum at 37 °C for up to 24 h (the time period investigated for serial PET imaging, which is about three half-lives of ^{66}Ga). Portions of the mixture were sampled at different time points and filtered through 100 kDa cutoff filters. The filtrates were collected and the radioactivity was measured. The percentages of retained ^{66}Ga on the GO conjugates (^{66}Ga-NOTA-GO-TRC105 or ^{66}Ga-NOTA-GO) were calculated using the following equation: (total radioactivity - radioactivity in filtrate)/total radioactivity.

2.7. PET and PET/CT imaging

PET scans were performed using an Inveon microPET/microCT rodent model scanner (Siemens Medical Solutions USA, Inc.) [27]. 4T1 tumor-bearing mouse was each injected with 5–10 MBq of ^{66}Ga-NOTA-GO-TRC105 or ^{66}Ga-NOTA-GO via tail vein and 5–15 minute static PET scans were performed at various time points post-injection (p.i.). A separate cohort of four 4T1 tumor-bearing mice was each injected with 2 mg of unlabeled TRC105 at 2 h before ^{66}Ga-NOTA-GO-TRC105 administration to evaluate the CD105 specificity of ^{66}Ga-NOTA-GO-TRC105 in vivo (i.e. blocking experiment).

Based on our previous experience with various radiolabeled nanomaterials [28–32] and taking into account the half-life of ^{66}Ga, the time points of 0.5, 3, 7, and 24 h p.i. were chosen for serial PET scans. PET images were reconstructed using a maximum a posteriori (MAP) algorithm, with no attenuation or scatter correction. For each microPET scan, 3-D regions-of-interest (ROIs) were drawn over the tumor and major organs with vendor software (Inveon Research Workplace [IRW]) on decay-corrected whole-body images. Assuming a tissue density of 1 g/mL, the ROIs were converted to MBq/g using a conversion factor (pre-determined using a 20 mL centrifuge tube filled with ~37 MBq of $^{66}GaCl_3$ as a phantom), and then divided by the total administered radioactivity to obtain an image ROI-derived percentage injected dose per gram of tissue (%ID/g). To anatomically localize the radioactivity signal observed in PET, a few animals were also subjected to microCT scans. Immediately after PET scanning, animals were transported to the microCT gantry, positioned, and scanned at a voxel resolution of 210 μm (scanning time: 7 min). Images were reconstructed using IRW and fiducial markers were used for co-registration.

2.8. Biodistribution study

Biodistribution studies were carried out to validate the %ID/g values obtained from non-invasive PET imaging against radioactivity distribution measured ex vivo. At 24 h p.i., mice were euthanized and blood, 4T1 tumor, and major organs/tissues were collected and wet-weighed. In addition, separate cohorts of 4T1 tumor-bearing mice were intravenously injected with ^{66}Ga-NOTA-GO-TRC105 or ^{66}Ga-NOTA-GO (four mice per group) and euthanized at 3 h p.i. (when tumor uptake was prominent based on PET results) for biodistribution studies. The radioactivity in each tissue was measured using a gamma-counter (Perkin Elmer) and presented as %ID/g (mean ± SD).

2.9. Histology

To confirm that tumor uptake of ^{66}Ga-NOTA-GO-TRC105 is CD105 specific and GO was indeed delivered to the tumor by TRC105, three 4T1 tumor-bearing mice were each injected with a larger dose of NOTA-GO-TRC105 (5 mg/kg mouse body weight) and euthanized at 3 h p.i. The 4T1 tumor, liver, spleen (i.e. tissues with significant uptake of ^{66}Ga-NOTA-GO-

TRC105), and muscle (which has negligible uptake of ^{66}Ga-NOTA-GO-TRC105 and serves as a control normal organ) were harvested, frozen, and cryo-sectioned for histological analysis.

Frozen tissue slices of 7 μm thickness were first visually inspected under a Nikon Eclipse Ti microscope for the presence of GO, without any immunofluorescence staining. Subsequently, the tissue slices were fixed with cold acetone and stained for endothelial marker CD31, as described previously through the use of a rat anti-mouse CD31 antibody and Cy3-labeled donkey anti-rat IgG [24, 25]. In addition, the tissue slices were incubated with 2 μg/mL of AlexaFluor488-labeled goat anti-human IgG for visualization of TRC105 on the NOTA-GO-TRC105. Of note, TRC105, within the NOTA-GO-TRC105 conjugate, served as the primary antibody for histological analysis of CD105 and no unconjugated TRC105 was used.

3. Results

3.1. Syntheses and characterization of GO conjugates

Schematic structures of the four GO conjugates are shown in Figure 1A. Based on AFM measurements, GO-PEG-NH_2, NOTA-GO, and NOTA-GO-TRC105 are all small sheets within a size range of 10 to 50 nm (Figure 1B), which was corroborated by DLS data that determined the average diameters of GO-PEG-NH_2, NOTA-GO, and NOTA-GO-TRC105 to be 21.7 ± 0.7 nm, 21.9 ± 0.6 nm, and 27.0 ± 0.9 nm, respectively. The zeta-potential values of GO-PEG-NH_2, NOTA-GO, and NOTA-GO-TRC105 were −4.85 ± 4.99 mV, −9.46 ± 4.74 mV, and −0.08 ± 5.35 mV, respectively. Together, the results from size and zeta-potential measurements indicated successful conjugation of NOTA and TRC105 onto GO.

3.2. Flow cytometry and serum stability studies

Treatment with FITC-GO-TRC105 greatly increased the mean fluorescence intensity of HUVECs (~600 fold higher than the untreated cells), whereas treatment with FITC-GO and the “blocking” group both exhibited little fluorescence increase (~100 fold lower than FITC-GO-TRC105, Figure 2A). These data demonstrated that FITC-GO-TRC105 specifically binds to CD105 on the HUVECs. Fluorescence signal on CD105 negative MCF-7 cells was minimal for all groups, indicating minimal non-specific binding of the covalently functionalized GO conjugates in cell culture. The CD105 specificity of FITC-GO-TRC105 in vitro warranted further in vivo investigation of NOTA-GO-TRC105.

More than 97% of ^{66}Ga remained on the GO conjugates over the 24 h incubation period (Figure 2B), indicating excellent stability of the ^{66}Ga-NOTA complex that was covalently conjugated to the GO surface through PEG chains. Since PET imaging detects the radiolabel (i.e. ^{66}Ga) instead of the GO conjugate per se, excellent stability of the radiolabel on the GO conjugates ensures that the signal observed by PET truly reflects distribution of the GO conjugates.

3.3. In vivo PET imaging and biodistribution studies

Coronal slices that contain the 4T1 tumor are shown in Figure 3A and representative PET/CT fused images of a mouse at 3 h p.i. of ^{66}Ga-NOTA-GO-TRC105 are shown in Figure 3B. Quantitative data obtained from ROI analysis of the PET results are shown in Figure 4. The GO conjugates investigated in this study were cleared primarily through the hepatobiliary pathway since their hydrodynamic diameter is significantly larger than the cutoff for renal filtration (~5 nm) [33]. Liver uptake of ^{66}Ga-NOTA-GO-TRC105 was 10.7 ± 1.7, 11.4 ± 1.5, 10.4 ± 1.3, and 8.0 ± 1.1 %ID/g at 0.5, 3, 7, and 24 h p.i respectively,

while the radioactivity in the blood was 10.9 ± 1.4, 7.5 ± 1.2, 5.3 ± 1.1, and 3.4 ± 0.4 %ID/g at 0.5, 3, 7, and 24 h p.i., respectively (n = 4; Figure 4A). Importantly, the 4T1 tumor accumulated ^{66}Ga-NOTA-GO-TRC105 very rapidly (clearly visible at 0.5 h p.i.) and the tumor uptake remained stable over time (3.8 ± 0.4, 4.5 ± 0.4, 5.8 ± 0.3, and 4.5 ± 0.4 %ID/g at 0.5, 3, 7, and 24 h p.i. respectively; n = 4; Figure 4A, D).

Administration of a blocking dose of TRC105 2 h before ^{66}Ga-NOTA-GO-TRC105 injection significantly reduced the tumor uptake to 1.3 ± 0.3, 1.5 ± 0.2, 1.1 ± 0.3, and 1.2 ± 0.1 %ID/g at 0.5, 3, 7, and 24 h p.i. respectively (n = 4; $P < 0.05$ at all time points examined when compared with mice injected with ^{66}Ga-NOTA-GO-TRC105 alone; Figure 3A, 4B,D), which clearly demonstrated CD105 specificity of ^{66}Ga-NOTA-GO-TRC105 in vivo. Liver uptake of ^{66}Ga-NOTA-GO-TRC105 in the “blocking” group was similar to mice injected with ^{66}Ga-NOTA-GO-TRC105 alone, which was9.0 ± 1.8, 10.8 ± 2.0, 10.0 ± 1.9, and 10.2 ± 1.9 %ID/g at 0.5, 3, 7, and 24 h p.i. respectively (n = 4). However, radioactivity in the blood (6.0 ± 1.2, 3.4 ± 0.8, 2.0 ± 0.3, and 2.0 ± 0.3 %ID/g at 0.5, 3, 7, and 24 h p.i. respectively; n = 4) was appreciably lower with a blocking dose of TRC105 (Figure 4B).

When compared with ^{66}Ga-NOTA-GO-TRC105, liver uptake of ^{66}Ga-NOTA-GO was similar, at 12.6 ± 2.1, 12.0 ± 1.8, 11.8 ± 1.9, and 11.7 ± 1.6 %ID/g at 0.5, 3, 7, and 24 h p.i. respectively (n = 4; Figure 4C). The radioactivity of ^{66}Ga-NOTA-GO in the blood was also comparable to ^{66}Ga-NOTA-GO-TRC105: 12.5 ± 2.2, 8.7 ± 1.5, 6.8 ± 1.1, and 3.5 ± 0.7 %ID/g at 0.5, 3, 7, and 24 h p.i. respectively (n = 4; Figure 4C). There was an appreciable level of ^{66}Ga-NOTA-GO uptake in the 4T1 tumor (2.9 ± 0.4, 3.2 ± 0.4, 3.6 ± 0.3, and 2.8 ± 0.2 %ID/g at 0.5, 3, 7, and 24 h p.i. respectively; n = 4; Figure 4C,D) attributed to the enhanced permeability and retention (EPR) effect alone. However, the %ID/g values were significantly lower than that of ^{66}Ga-NOTA-GO-TRC105 ($P < 0.05$) at all time points examined, which confirmed that conjugation of TRC105 was the critical factor for enhanced tumor uptake of GO conjugates.

After the terminal PET scans at 24 h p.i., biodistribution studies were carried out. In addition, separate groups of four 4T1 tumor-bearing mice were each intravenously injected with ^{66}Ga-NOTA-GO-TRC105 or ^{66}Ga-NOTA-GO and euthanized at 3 h p.i. for biodistribution studies. The liver, spleen and blood had significant radioactivity accumulation at 3 h p.i. for both ^{66}Ga-NOTA-GO-TRC105 and ^{66}Ga-NOTA-GO (Figure 5A). Importantly, uptake of ^{66}Ga-NOTA-GO-TRC105 in the 4T1 tumor was higher than all other major organs, thus providing good tumor contrast. The biodistribution of ^{66}Ga-NOTA-GO-TRC105 and ^{66}Ga-NOTA-GO was similar in most normal tissues except the 4T1 tumor, for which the difference in uptake of ^{66}Ga-NOTA-GO-TRC105 and ^{66}Ga-NOTA-GO reached statistical significance and confirmed CD105 specificity of ^{66}Ga-NOTA-GO-TRC105. Overall, the quantitative data obtained from non-invasive PET (Figure 4) and ex vivo biodistribution (Figure 5) studies were in good agreement.

3.4. Histology

Micrographs of the tissue slices clearly showed that there were significant amount of NOTA-GO-TRC105 in the tumor, liver, and spleen, but not in muscle (dark spots in Figure 6A). However, there was no observable GO in the tumor of mice injected with NOTA-GO. Therefore, both the ^{66}Ga (detected by PET) and GO (visible under the microscope) were delivered to the 4T1 tumor by TRC105-based CD105 targeting, which confirmed good in vivo stability of ^{66}Ga-NOTA-GO-TRC105 and corroborated the serum stability results. The histology findings also demonstrated that NOTA-GO-TRC105 specifically targets CD105 in the tumor vasculature. As can be seen in Figure 6B, NOTA-GO-TRC105 distribution in the 4T1 tumor was primarily on the tumor vasculature (indicated by good overlay of the red and green fluorescence signal, which represents CD31 and CD105 respectively) with little

extravasation. Taken together the results from micrographs and immunofluorescence images, our observations suggested that NOTA-GO-TRC105 was quite stable in vivo and was specifically directed to the tumor vasculature as an intact entity through targeting CD105 on the tumor neovasculature, with little extravasation.

Prominent fluorescence signal in the liver and spleen slices, resulting from TRC105 within NOTA-GO-TRC105, indicated significant uptake of NOTA-GO-TRC105 by these two organs, which is consistent with the PET/biodistribution findings. However, the green fluorescence attributed to NOTA-GO-TRC105 had little overlay with CD31 staining of vessels in the liver and spleen, manifesting that the uptake of NOTA-GO-TRC105 in these two organs was primarily due to non-specific capture by the reticuloendothelial system instead of specific targeting of CD105 on the vasculature. Meanwhile, little signal originating from NOTA-GO-TRC105 was observed in normal tissues such as the muscle, which is consistent with the in vivo imaging results.

4. Discussion

In this work, we have investigated the in vivo behavior of covalently functionalized GO conjugates in the 4T1 tumor model with ^{66}Ga-based PET imaging. The significance of this study lies in several aspects. First, in vivo active tumor targeting of graphene has not been reported to date by other research groups. Achieving active tumor targeting and imaging in vivo is an important advance in the emerging field of graphene-based nanomedicine. The significantly improved tumor targeting efficiency of nano-graphene realized in this work may be utilized for future molecularly-targeted drug delivery and/or photothermal therapy of cancer, to further enhance therapeutic efficacy and enable cancer theranostics. The versatile chemistry of graphene-based nanomaterials makes them attractive nanoplatforms for future biomedical research.

Second, past work with ^{66}Ga has been very limited due to the relatively low specific activities achieved using reported methods (< 4.6 GBq/μmol of chelator [15]), which were several orders of magnitude below the theoretical limit and might affect the tracer uptake due to excessive injected mass, as well as the significant number of high energy gammas and positrons characteristic of its decay. Recently, we were able to produce ^{66}Ga with reactivities for NOTA approaching 740 GBq/μmol (i.e. 20 Ci/μmol) using isotope-enriched ^{66}Zn, or > 74 GBq/μmol (i.e. 2 Ci/μmol) using natural Zn as the cyclotron target [14]. ^{68}Ga, another commonly used PET isotope of gallium, has been used to label a wide variety of compounds and sets the stage for future investigation of these compounds with the longer-lived ^{66}Ga. For example, many tracers (some are currently in clinical investigation) can only be imaged with PET within a few hours after injection due to the short half-life of ^{68}Ga. The use of ^{66}Ga can allow for PET imaging at later time points to evaluate the long term fate of these tracers, which may provide more biological insights in therapeutic intervention and/or tumor development.

PET has been widely used in clinical oncology for cancer staging and monitoring the therapeutic response [34–37]. Modern preclinical PET scanners can capably cope with both fast positrons and prompt gamma emissions characteristic of many non-standard radionuclides, including ^{68}Ga and ^{66}Ga [38, 39]. Although ^{66}Ga has higher positron energy (E_{max} of 4.15 MeV) than other commonly used PET isotopes (e.g. E_{max} of 0.64 MeV for ^{18}F and 0.97 MeV for ^{11}C, respectively) [40, 41], high energy positrons and co-emitted gammas only had a small effect on the ultimate PET image quality and quantitation accuracy in our study, further enabling researchers to consider future use of the versatile radiometal for PET.

Robust chemistry for both radiolabeling and targeting ligand conjugation is of critical importance to future applications of radiolabeled nanomaterials. For imaging applications, the stability of the radioisotope(s) on the nanomaterial should always be confirmed, otherwise the imaging results may be irrelevant to the actual nanomaterial distribution. The stability of NOTA as a chelator for radiogallium has been well documented in the literature [16]. As revealed by the in vitro studies, excellent serum stability of ^{66}Ga-NOTA-GO-TRC105 validated ^{66}Ga as a highly competitive candidate for nanomaterial labeling in the future. Besides the significantly higher specific activity of ^{66}Ga than many other commonly used radiometals such as ^{64}Cu and ^{89}Zr, the high energy positron emission (although not ideal for PET imaging) also makes ^{66}Ga a desirable isotope for Cerenkov luminescence imaging, a research topic that is currently under active investigation [42].

There are many challenges facing future biomedical applications of radiolabeled nanomaterials, and one of the key hurdles is (tumor) targeting efficacy. The majority of reports on radiolabeled nanomaterials to date utilized passive targeting only based on the EPR effect, which relies on the long circulation half-lives of the nanomaterials (liposomes in most cases) [21]. However, tumor targeting based on the EPR effect alone is far from ideal. We believe that tumor vasculature targeting is a promising approach for radiolabeled nanomaterials since many of these nanomaterials are too large to extravasate [28, 43–45]. The vascular target of our study, CD105, is primarily present on the tumor neovasculature. Even though the 4T1 tumor cells are CD105 negative per se, as demonstrated in our previous studies [24, 25, 46], they grow rapidly when inoculated into mice and contain a highly angiogenic tumor vasculature with high CD105 expression. This study confirmed that CD105 is a suitable target for further increasing the tumor uptake of GO conjugates through the incorporation of TRC105, a high affinity mAb that binds to CD105.

5. Conclusion

Herein we demonstrated that GO can be specifically directed to the tumor neovasculature in vivo through targeting of CD105, a vascular marker for tumor angiogenesis. The covalently functionalized GO exhibited excellent stability and target specificity. Pharmacokinetics and tumor targeting efficacy of ^{66}Ga-NOTA-GO-TRC105 were investigated with both serial non-invasive PET imaging and biodistribution studies, which were validated with various in vitro/in vivo/ex vivo experiments. It was found that tumor targeting of NOTA-GO-TRC105 was vasculature specific with little extravasation.

Acknowledgments

This work is supported, in part, by the University of Wisconsin Carbone Cancer Center, the Department of Defense (W81XWH-11-1-0644 and W81XWH-11-1-0648), NCRR 1UL1RR025011, and the NIH through the UW Radiological Sciences Training Program 5 T32 CA009206-32. The authors thank Dr.s Kai Yang and Zhuang Liu from Soochow University for providing the nano-graphene. CPT is an employee and shareholder of TRACON Pharmaceuticals, Inc.

References

1. Novoselov KS, Geim AK, Morozov SV, Jiang D, Zhang Y, Dubonos SV, et al. Electric field effect in atomically thin carbon films. Science. 2004; 306:666–9. [PubMed: 15499015]
2. Feng L, Liu Z. Graphene in biomedicine: opportunities and challenges. Nanomedicine (Lond). 2011; 6:317–24. [PubMed: 21385134]
3. Zhu Y, Murali S, Cai W, Li X, Suk JW, Potts JR, et al. Graphene and graphene oxide: synthesis, properties, and applications. Adv Mater. 2010; 22:3906–24. [PubMed: 20706983]
4. Li X, Wang X, Zhang L, Lee S, Dai H. Chemically derived, ultrasmooth graphene nanoribbon semiconductors. Science. 2008; 319:1229–32. [PubMed: 18218865]

5. Liu Z, Robinson JT, Sun X, Dai H. PEGylated nanographene oxide for delivery of water- insoluble cancer drugs. J Am Chem Soc. 2008; 130:10876–7. [PubMed: 18661992]
6. Tian B, Wang C, Zhang S, Feng L, Liu Z. Photothermally enhanced photodynamic therapy delivered by nano-graphene oxide. ACS Nano. 2011; 5:7000–9. [PubMed: 21815655]
7. Feng L, Zhang S, Liu Z. Graphene based gene transfection. Nanoscale. 2011; 3:1252–7. [PubMed: 21270989]
8. Yang K, Zhang S, Zhang G, Sun X, Lee ST, Liu Z. Graphene in mice: ultrahigh in vivo tumor uptake and efficient photothermal therapy. Nano Lett. 2010; 10:3318–23. [PubMed: 20684528]
9. Zhang W, Guo Z, Huang D, Liu Z, Guo X, Zhong H. Synergistic effect of chemo-photothermal therapy using PEGylated graphene oxide. Biomaterials. 2011; 32:8555–61. [PubMed: 21839507]
10. Yang K, Wan J, Zhang S, Zhang Y, Lee ST, Liu Z. In vivo pharmacokinetics, long-term biodistribution, and toxicology of PEGylated graphene in mice. ACS Nano. 2011; 5:516–22. [PubMed: 21162527]
11. Duch MC, Budinger GR, Liang YT, Soberanes S, Urich D, Chiarella SE, et al. Minimizing Oxidation and Stable Nanoscale Dispersion Improves the Biocompatibility of Graphene in the Lung. Nano Lett. 2011; 11:5201–7. [PubMed: 22023654]
12. Ruiz ON, Fernando KA, Wang B, Brown NA, Luo PG, McNamara ND, et al. Graphene oxide: a nonspecific enhancer of cellular growth. ACS Nano. 2011; 5:8100–7. [PubMed: 21932790]
13. Li Y, Liu Y, Fu Y, Wei T, Le Guyader L, Gao G, et al. The triggering of apoptosis in macrophages by pristine graphene through the MAPK and TGF-beta signaling pathways. Biomaterials. 2012; 33:402–11. [PubMed: 22019121]
14. Engle JW, Lopez-Rodriguez V, Gaspar-Carcamo RE, Valdovinos HF, Valle-Gonzalez M, Trejo-Ballado F, et al. Very high specific activity $^{66/68}$Ga from zinc targets for PET. Appl Radiat Isot Revision.
15. Lewis MR, Reichert DE, Laforest R, Margenau WH, Shefer RE, Klinkowstein RE, et al. Production and purification of gallium-66 for preparation of tumor-targeting radiopharmaceuticals. Nucl Med Biol. 2002; 29:701–6. [PubMed: 12234596]
16. Velikyan I. Positron emitting ^{68}Ga-based imaging agents: chemistry and diversity. Med Chem. 2011; 7:345–79. [PubMed: 21711223]
17. Seon BK, Haba A, Matsuno F, Takahashi N, Tsujie M, She X, et al. Endoglin-targeted cancer therapy. Curr Drug Deliv. 2011; 8:135–43. [PubMed: 21034418]
18. Zhang Y, Yang Y, Hong H, Cai W. Multimodality molecular imaging of CD105 (Endoglin) expression. Int J Clin Exp Med. 2011; 4:32–42. [PubMed: 21394284]
19. Fonsatti E, Nicolay HJ, Altomonte M, Covre A, Maio M. Targeting cancer vasculature via endoglin/CD105: a novel antibody-based diagnostic and therapeutic strategy in solid tumours. Cardiovasc Res. 2010; 86:12–9. [PubMed: 19812043]
20. Dallas NA, Samuel S, Xia L, Fan F, Gray MJ, Lim SJ, et al. Endoglin (CD105): a marker of tumor vasculature and potential target for therapy. Clin Cancer Res. 2008; 14:1931–7. [PubMed: 18381930]
21. Hong H, Zhang Y, Sun J, Cai W. Molecular imaging and therapy of cancer with radiolabeled nanoparticles. Nano Today. 2009; 4:399–413. [PubMed: 20161038]
22. Ruoslahti E, Bhatia SN, Sailor MJ. Targeting of drugs and nanoparticles to tumors. J Cell Biol. 2010; 188:759–68. [PubMed: 20231381]
23. Mendelson DS, Gordon MS, Rosen LS, Hurwitz H, Wong MK, Adams BJ, et al. Phase I study of TRC105 (anti-CD105 [endoglin] antibody) therapy in patients with advanced refractory cancer. J Clin Oncol. 2010; 28:15s.
24. Hong H, Yang Y, Zhang Y, Engle JW, Barnhart TE, Nickles RJ, et al. Positron emission tomography imaging of CD105 expression during tumor angiogenesis. Eur J Nucl Med Mol Imaging. 2011; 38:1335–43. [PubMed: 21373764]
25. Yang Y, Zhang Y, Hong H, Liu G, Leigh BR, Cai W. In vivo near-infrared fluorescence imaging of CD105 expression. Eur J Nucl Med Mol Imaging. 2011; 38:2066–76. [PubMed: 21814852]
26. Takahashi N, Haba A, Matsuno F, Seon BK. Antiangiogenic therapy of established tumors in human skin/severe combined immunodeficiency mouse chimeras by anti-endoglin (CD105)

monoclonal antibodies, and synergy between anti-endoglin antibody and cyclophosphamide. Cancer Res. 2001; 61:7846–54. [PubMed: 11691802]

27. Zhang Y, Hong H, Engle JW, Yang Y, Barnhart TE, Cai W. Positron emission tomography and near-infrared fluorescence imaging of vascular endothelial growth factor with dual-labeled bevacizumab. Am J Nucl Med Mol Imaging. 2012; 2:1–13. [PubMed: 22229128]
28. Cai W, Chen K, Li ZB, Gambhir SS, Chen X. Dual-function probe for PET and near- infrared fluorescence imaging of tumor vasculature. J Nucl Med. 2007; 48:1862–70. [PubMed: 17942800]
29. Chen K, Li ZB, Wang H, Cai W, Chen X. Dual-modality optical and positron emission tomography imaging of vascular endothelial growth factor receptor on tumor vasculature using quantum dots. Eur J Nucl Med Mol Imaging. 2008; 35:2235–44. [PubMed: 18566815]
30. Liu Z, Cai W, He L, Nakayama N, Chen K, Sun X, et al. *In vivo* biodistribution and highly efficient tumour targeting of carbon nanotubes in mice. Nat Nanotechnol. 2007; 2:47–52. [PubMed: 18654207]
31. Hong H, Shi J, Yang Y, Zhang Y, Engle JW, Nickles RJ, et al. Cancer-targeted optical imaging with fluorescent zinc oxide nanowires. Nano Lett. 2011; 11:3744–50. [PubMed: 21823599]
32. Yang X, Hong H, Grailer JJ, Rowland IJ, Javadi A, Hurley SA, et al. cRGD-functionalized, DOX-conjugated, and ^{64}Cu-labeled superparamagnetic iron oxide nanoparticles for targeted anticancer drug delivery and PET/MR imaging. Biomaterials. 2011; 32:4151–60. [PubMed: 21367450]
33. Choi HS, Liu W, Misra P, Tanaka E, Zimmer JP, Itty Ipe B, et al. Renal clearance of quantum dots. Nat Biotechnol. 2007; 25:1165–70. [PubMed: 17891134]
34. Gambhir SS. Molecular imaging of cancer with positron emission tomography. Nat Rev Cancer. 2002; 2:683–93. [PubMed: 12209157]
35. Eary JF, Hawkins DS, Rodler ET, Conrad EUI. ^{18}F-FDG PET in sarcoma treatment response imaging. Am J Nucl Med Mol Imaging. 2011; 1:47–53.
36. Iagaru A. ^{18}F-FDG PET/CT: timing for evaluation of response to therapy remains a clinical challenge. Am J Nucl Med Mol Imaging. 2011; 1:63–4.
37. Vach W, Høilund-Carlsen PF, Fischer BM, Gerke O, Weber W. How to study optimal timing of PET/CT for monitoring of cancer treatment. Am J Nucl Med Mol Imaging. 2011; 1:54–62.
38. Laforest R, Rowland DJ, Welch MJ. MicroPET imaging with nonconventional isotopes. IEEE Trans Nucl Sci. 2002; 49:2119–26.
39. Graham MC, Pentlow KS, MAwlawi O, Finn RD, Daghighian F, Larson SM. An investigationof the physical characteristics of ^{66}Ga an an isotope for PET imaging and quantification. Med Phys. 1997; 24:317–27. [PubMed: 9048374]
40. Alauddin MM. Positron emission tomography (PET) imaging with ^{18}F-based radiotracers. Am J Nucl Med Mol Imaging. 2012; 2:55–76.
41. Grassi I, Nanni C, Allegri V, Morigi JJ, Montini GC, Castellucci P, et al. The clinical use of PET with ^{11}C-acetate. Am J Nucl Med Mol Imaging. 2012; 2:33–47.
42. Ruggiero A, Holland JP, Lewis JS, Grimm J. Cerenkov luminescence imaging of medical isotopes. J Nucl Med. 2010; 51:1123–30. [PubMed: 20554722]
43. Cai W, Chen X. Preparation of peptide conjugated quantum dots for tumour vasculature targeted imaging. Nat Protoc. 2008; 3:89–96. [PubMed: 18193025]
44. Cai W, Chen X. Multimodality molecular imaging of tumor angiogenesis. J Nucl Med. 2008; 49 (Suppl 2):113S–28S. [PubMed: 18523069]
45. Cai W, Shin DW, Chen K, Gheysens O, Cao Q, Wang SX, et al. Peptide-labeled near-infrared quantum dots for imaging tumor vasculature in living subjects. Nano Lett. 2006; 6:669–76. [PubMed: 16608262]
46. Hong H, Severin GW, Yang Y, Engle JW, Zhang Y, Barnhart TE, et al. Positron emission tomography imaging of CD105 expression with ^{89}Zr-Df-TRC105. Eur J Nucl Med Mol Imaging. 2012; 39:138–48. [PubMed: 21909753]

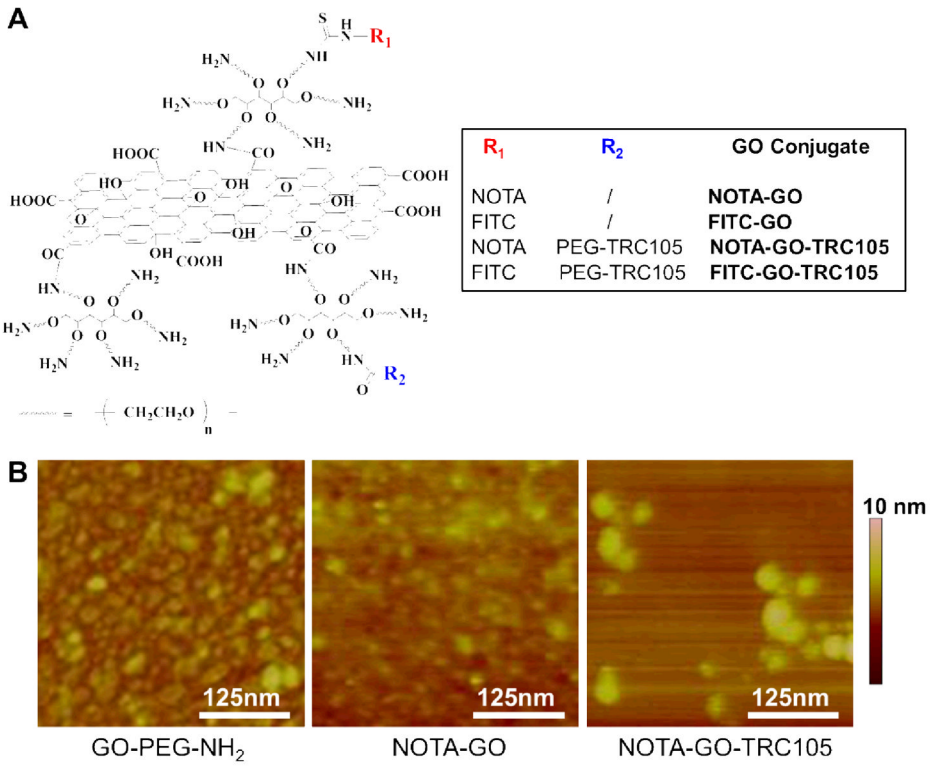

R_1	R_2	GO Conjugate
NOTA	/	**NOTA-GO**
FITC	/	**FITC-GO**
NOTA	PEG-TRC105	**NOTA-GO-TRC105**
FITC	PEG-TRC105	**FITC-GO-TRC105**

Fig. 1.

A schematic representation of the four nano-graphene conjugates use in this study (**A**) and representative atomic force microscopy images of the conjugates (**B**).

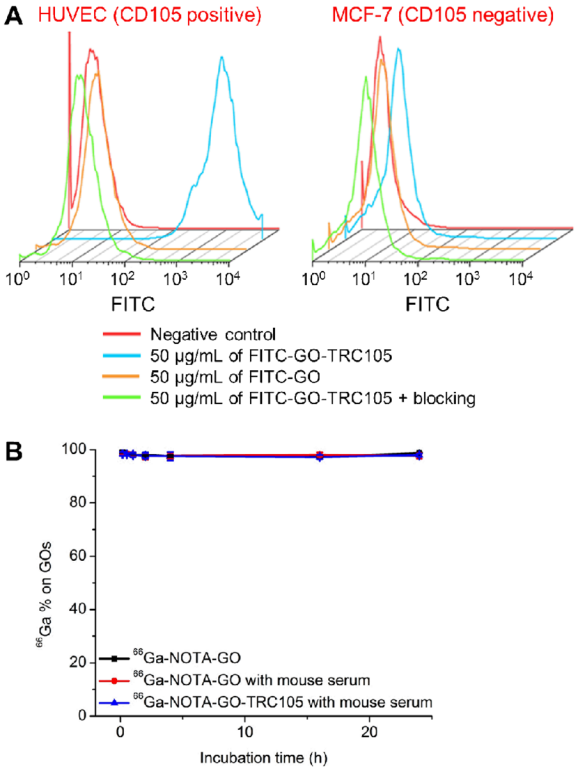

Fig. 2.

In vitro characterization of the GO conjugates. (**A**) Flow cytometry analysis of the GO conjugates in HUVECs (CD105 positive) and MCF-7 breast cancer cells (CD105 negative). (**B**) Serum stability studies showed that the vast majority of ^{66}Ga remains intact on the GO after incubation in complete mouse serum at 37 °C for 24 h.

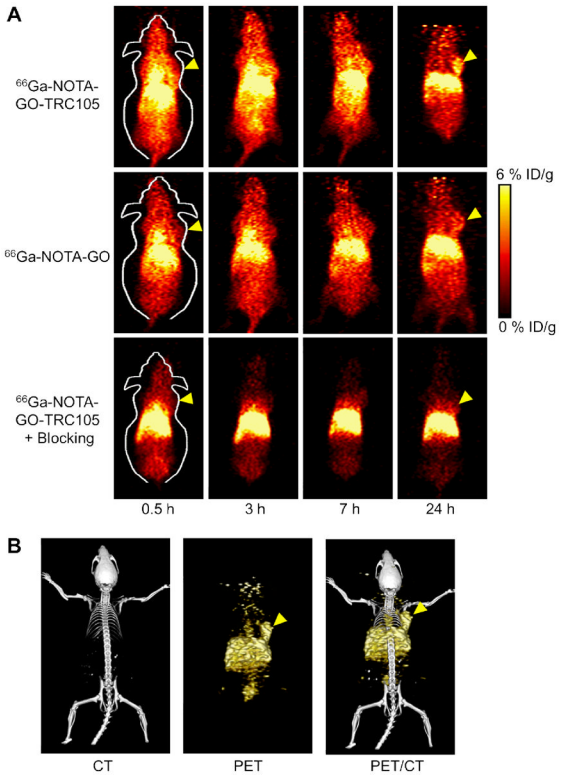

Fig. 3.

In vivo PET/CT imaging of ^{66}Ga-labeled GO conjugates in 4T1 tumor-bearing mice. (**A**) Serial coronal PET images of 4T1 tumor-bearing mice at different time points post-injection of ^{66}Ga-NOTA-GO-TRC105, ^{66}Ga-NOTA-GO, or ^{66}Ga-NOTA-GO-TRC105 at 2 h after a blocking dose of TRC105 (denoted as “blocking”). (**B**) Representative PET/CT images of ^{66}Ga-NOTA-GO-TRC105 in 4T1 tumor-bearing mice at 3 h post-injection. Tumors are indicated by arrowheads.

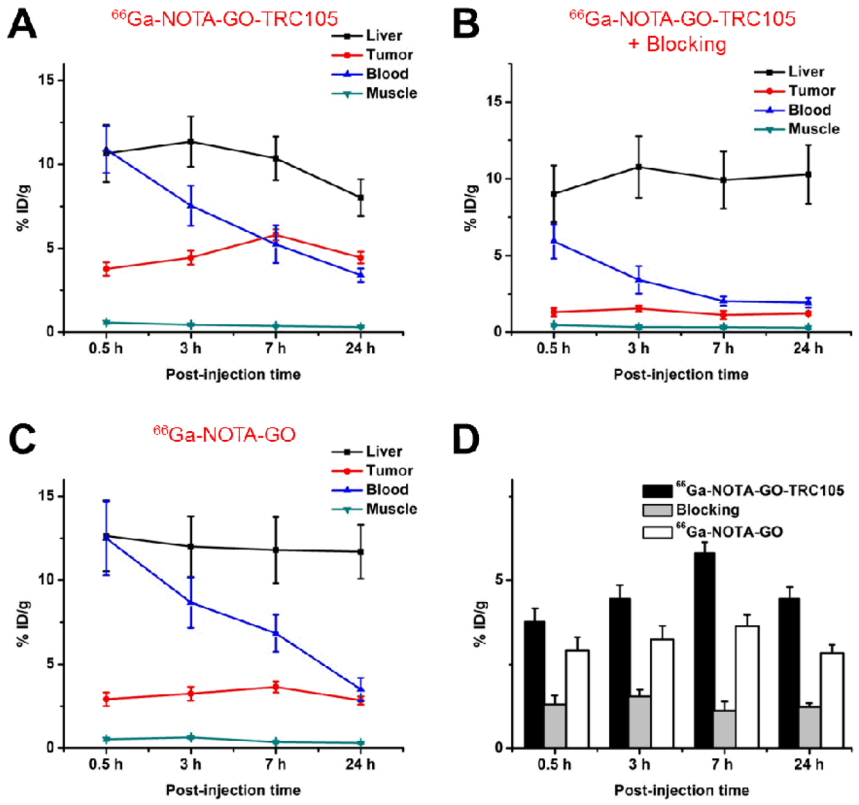

Fig. 4.

Quantitative analysis of the PET data. (**A**) Time-activity curves of the liver, 4T1 tumor, blood, and muscle upon intravenous injection of ^{66}Ga-NOTA-GO-TRC105. (**B**) Time-activity curves of the liver, 4T1 tumor, blood, and muscle upon intravenous injection of ^{66}Ga-NOTA-GO-TRC105, after a blocking dose of TRC105. (**C**) Time-activity curves of the liver, 4T1 tumor, blood, and muscle upon intravenous injection of ^{66}Ga-NOTA-GO. (**D**) Comparison of the 4T1 tumor uptake in the three groups. The differences between 4T1 tumor uptake of ^{66}Ga-NOTA-GO-TRC105 and the two control groups were statistically significant ($P < 0.05$) at all time points examined. All data represent 4 mice per groups.

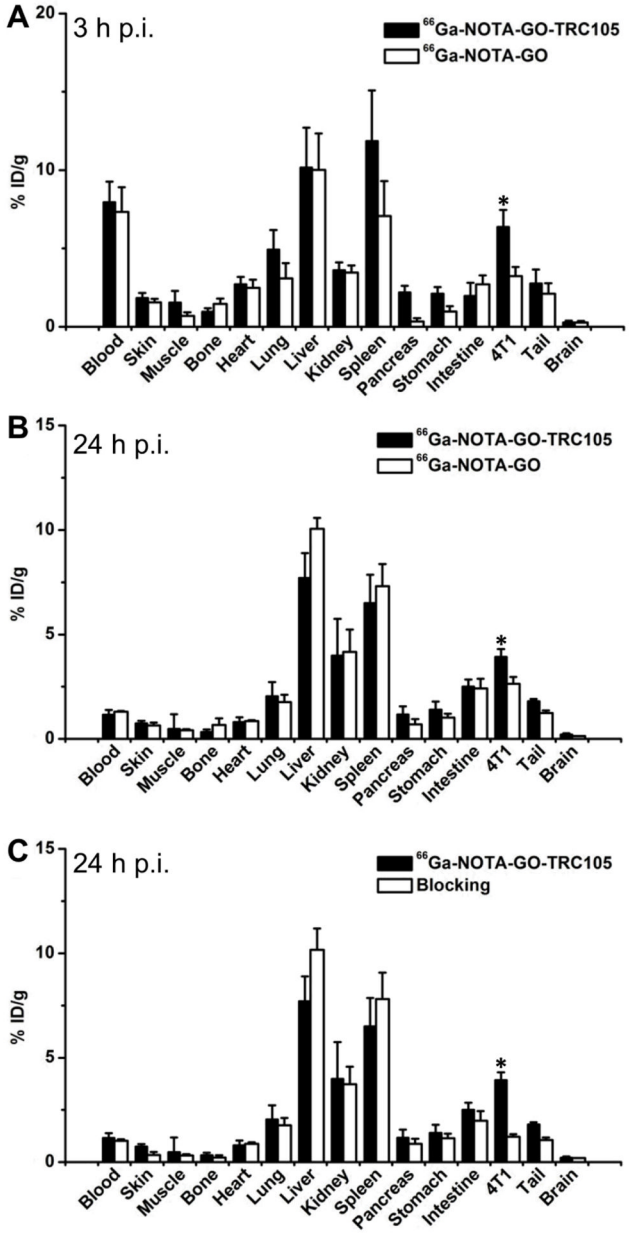

Fig. 5.

Biodistribution studies in 4T1 tumor-bearing mice. (**A**) Biodistribution of ^{66}Ga-NOTA-GO-TRC105 and ^{66}Ga-NOTA-GO in 4T1 tumor-bearing mice at 3 h post-injection. (**B**) Biodistribution of ^{66}Ga-NOTA-GO-TRC105 and ^{66}Ga-NOTA-GO in 4T1 tumor-bearing mice at 24 h post-injection. (**C**) Biodistribution of ^{66}Ga-NOTA-GO-TRC105 and ^{66}Ga-NOTA-GO-TRC105 after a blocking dose of TRC105 (i.e. blocking) in 4T1 tumor-bearing mice at 24 h post-injection. All data represent 4 mice per group. *: $p < 0.05$.

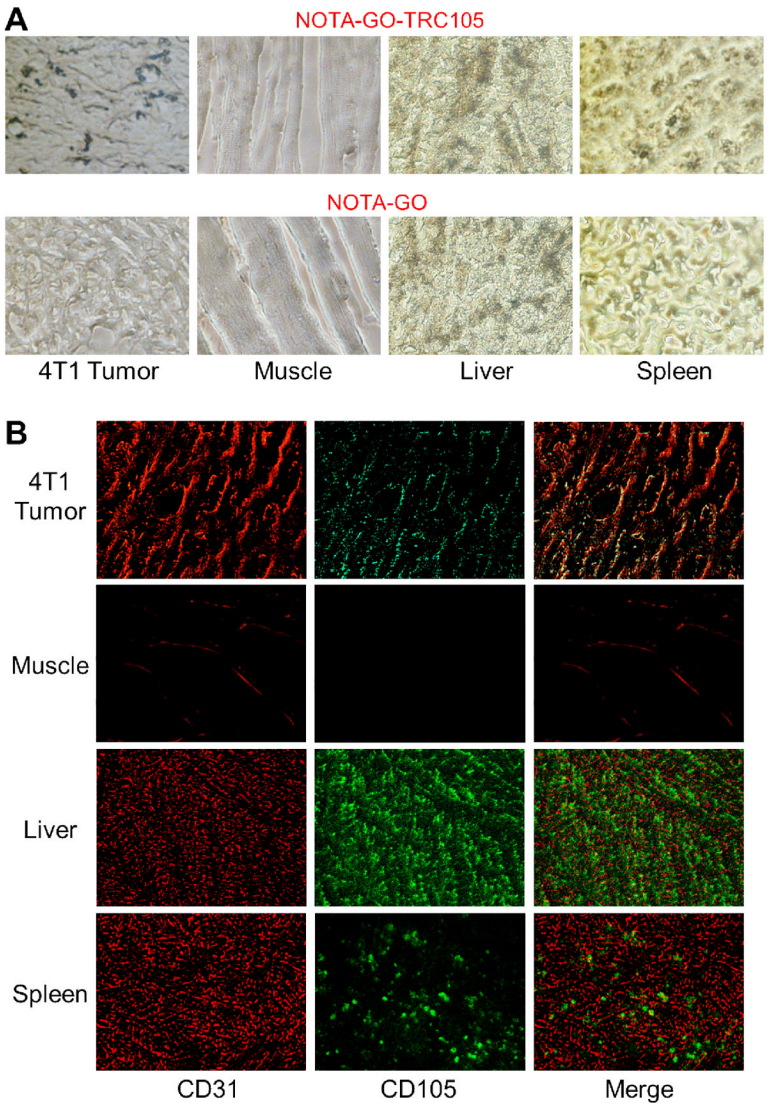

Fig. 6.

Ex vivo histological analysis. (**A**) Micrographs of tissue slices harvested from mice injected with NOTA-GO-TRC105 or NOTA-GO. The dark spots indicate the presence of GO. (**B**) Immunofluorescence staining of the tissue slices for CD31 (red, with anti-mouse CD31 primary antibody) and CD105 (green, using the TRC105 within NOTA-GO-TRC105 as the primary antibody). Merged images are also shown.